# Intraseasonal Teleconnection between North American and Western North Pacific Monsoons with 20-Day Time Scale

XIANAN JIANG

*Atmospheric and Oceanic Sciences Program, Princeton University, Princeton, New Jersey*

NGAR-CHEUNG LAU

*NOAA/Geophysical Fluid Dynamics Laboratory, Princeton University, Princeton, New Jersey*

(Manuscript received 2 May 2007, in final form 8 August 2007)

ABSTRACT

Based on a recently released, high-resolution reanalysis dataset for the North American region, the intraseasonal variability (ISV; with a time scale of about 20 days) of the North American monsoon (NAM) is examined. The rainfall signals associated with this phenomenon first emerge near the Gulf of Mexico and eastern Pacific at about 20°N. They subsequently migrate to the southwestern United States along the slope of the Sierra Madre Occidental. The rainfall quickly dissipates upon arrival at the desert region of Arizona and New Mexico (AZNM). The enhanced rainfall over AZNM is accompanied by strong southeasterly low-level flow along the Gulf of California. This pattern bears strong resemblance to the circulation related to "gulf surge" events, as documented by many studies. The southeasterly flow is associated with an anomalous low vortex over the subtropical eastern Pacific Ocean off California, and a midlatitude anticyclone over the central United States in the lower troposphere. This flow pattern is in broad agreement with that favoring the "wet surges" over the southwestern United States.

It is further demonstrated that the aforementioned low-level circulations associated with ISV of the NAM are part of a prominent trans-Pacific wave train extending from the western North Pacific (WNP) to the Eastern Pacific/North America along a "great circle" path. The circulation anomalies along the axis of this wave train exhibit a barotropic vertical structure over most regions outside of the WNP, and a baroclinic structure over the WNP, thus suggesting the important role of convective activities over the WNP in sustaining this wave train. This inference is further substantiated by an analysis of the pattern of wave-activity–flux vectors. Variations in the WNP convection are correlated with the ISV of the monsoons in both North American and East Asian (EA)/WNP sectors. These relationships lead to notable teleconnections between NAM and the EA/WNP monsoon on 20-day time scales.

## 1. Introduction

A significant summer monsoon prevails over northwestern Mexico and the southwestern United States (e.g., see Tang and Reiter 1984). In particular, the seasonal march of precipitation over Arizona and western New Mexico, which are situated in the northern portion of the North American monsoon (NAM) region, is characterized by an extremely dry June, followed by summer rains lasting from July until mid-September, and the reestablishment of a drier regime thereafter. The summertime rainfall (July through September) associated with the NAM accounts for at least 50% (40%) of the annual rainfall for northwestern Mexico (southern Arizona/New Mexico; Douglas et al. 1993; Adams and Comrie 1997). Hence the NAM exerts profound societal and economic impacts on this region.

The onset of the summer monsoon rainfall over southwestern North America has been linked to a decrease of rainfall over the U.S. Great Plains, and to an increase of rainfall along the Atlantic seaboard (Douglas et al. 1993; Higgins et al. 1997). Seasonal phase reversals in this continental-scale precipitation pattern are found to be associated with changes in the NAM intensity (Okabe 1995). Therefore, as one of the active components of the climate system over North America during the warm season, the NAM plays an important

*Corresponding author address:* Dr. Xianan Jiang, Jet Propulsion Laboratory, California Institute of Technology, MS 183-501, 4800 Oak Grove Drive, Pasadena, CA 91109.
E-mail: xianan@caltech.edu

DOI: 10.1175/2007JCLI2024.1

role in the climate variability in that region. A better understanding of this phenomenon is essential for improving our skill in making predictions of the weather and climate over North America. Various facets of the NAM system have been examined in detail during the North American Monsoon Experiment launched in summer 2004 (Higgins et al. 2006).

While the active/break cycles of summer monsoon over the Asian continent have been intensively investigated during the past decades (e.g., Sikka and Gadgil 1980; Lau and Chan 1986), studies on the variability of the NAM remain rather limited. The difficulty in understanding the variability of summertime convective activity in the southwestern United States and northwestern Mexico may partially be attributed to the extremely complicated topography in this region. Previous diagnostic and modeling studies suggest that the NAM rainfall is frequently modulated by "gulf surge" events along the Gulf of California (GoC). The gulf surges, initially described by Hales (1972), are northward surges of relatively cool and moist maritime air from the ocean to the southwestern arid region of the United States (Stensrud et al. 1997; Fuller and Stensrud 2000; Higgins et al. 2004; Bordoni et al. 2004). It has been further illustrated that a strong surge event is accompanied by the passage of a midlatitude trough across the western United States, and is also preceded by the propagation of tropical easterly waves across western Mexico several days earlier (Stensrud et al. 1997; Fuller and Stensrud 2000). By using near-surface Quick Scatterometer (QuikSCAT) winds derived from satellite observations, Bordoni and Stevens (2006) found that, although the gulf surges are mostly confined to the GoC and exhibit mesoscale characteristics, they are also intimately linked to patterns of large-scale variability.

Most of the previous studies are focused on the mesoscale features associated with NAM rainfall with time scales of several days. The intraseasonal variability (ISV) of the NAM has received relatively less attention. Mo and Higgins (1998) have examined the covariability of precipitation regimes over the western United States and convection in the tropical western Pacific on intraseasonal and interannual time scales. More recently, Lorenz and Hartmann (2006) proposed that the eastward-propagating Madden–Julian oscillation (MJO) along the equator could exert a significant impact on ISV of rainfall over the NAM region by modulating activities of synoptic systems over the eastern equatorial Pacific, including easterly waves, tropical storms, and surge events over the GoC. Higgins et al. (2004), however, indicated that the moisture surges over the GoC may not necessarily lead to enhanced rainfall over the NAM region. Furthermore, Mo and Nogues-Paegle (2005) noted only a weak influence of the MJO on summertime rainfall over the southwestern United States. The dominant mode that affects active and break periods of rainfall over the southwestern United States has a time scale of 20–28 days (Mo 2000). A characteristic time scale of about 20 days for rainfall variability over the southwestern United States has also been reported by Mullen et al. (1998) and Kiladis and Hall-McKim (2004). These time scales are somewhat shorter than that typically associated with the MJO. Kiladis and Hall-McKim (2004) have further linked enhanced NAM rainfall episodes to a large-scale circulation pattern associated with Rossby wave energy propagation from the North Pacific to North America several days earlier. Apparently, still more efforts are needed to improve our understanding of the physical mechanisms responsible for ISV of NAM rainfall.

By capitalizing on the recent release of a high-resolution reanalysis dataset for the North American sector, we have made an attempt in this study to examine in greater detail the essential features associated with ISV of rainfall over the NAM region. Our primary goal is to make use of these new findings to expand our knowledge of the physical processes contributing to ISV of the NAM. We have also broadened our investigation to include teleconnections between variability in the NAM region and circulation changes in other parts of the globe, particularly those occurring in the tropical western North Pacific (WNP) and East Asia. The organization of this paper is as follows: the datasets employed in this study are described in section 2. In section 3, we present results on ISV of rainfall and circulation in the vicinity of North America using regional reanalysis data. Then the global-scale aspects of atmospheric changes associated with ISV of NAM rainfall are examined in section 4. Finally, a discussion on the possible mechanisms responsible for ISV of the NAM and a summary of the principal findings are offered in section 5.

## 2. Data and methodology

The primary observational database for this study is the archive generated by the North American Regional Reanalysis (NARR) project for the 1979–2001 period. This is a long-term, consistent, high-resolution (32 km, 45 layer, 3 hourly) climate dataset for North America (Mesinger et al. 2006). The precipitation field in this reanalysis dataset over the continental United States is in good agreement with station observations. Temperature and vector wind are also considerably improved over the corresponding fields in the global National

Centers for Environmental Prediction (NCEP) reanalyses throughout the troposphere (Mesinger et al. 2006). For the purpose of examining ISV of the NAM rainfall and associated large-scale circulation features, daily averaged data for precipitation rate, wind, geopotential height, and specific humidity at 29 pressure levels are used in this study.

To determine the linkage of the global circulation pattern to ISV of rainfall over the NAM region, the 40-yr European Centre for Medium-Range Weather Forecasts (ECMWF) Re-Analyses (ERA-40) are examined. The variables of interest include wind, geopotential height, and temperature at 12 pressure levels. In addition, the outgoing longwave radiation (OLR; Liebmann and Smith 1996) data processed by the National Oceanic and Atmospheric Administration (NOAA) are also employed as the proxy for tropical convection. Both the ERA-40 and OLR datasets are daily averages, with global coverage at a latitudinal and longitudinal resolution of 2.5°.

The results in the following sections are based on diagnoses of various data fields for the NAM summer season (June–August) in the 1979–2001 period. The mean seasonal cycle in the raw data is removed by subtracting the time mean and first six harmonics of climatological annual cycle based on 23-yr averages. Since this study is primarily concerned with fluctuations on intraseasonal time scales, the interannual variability is further removed by subtracting the seasonal-mean anomaly for a given year from the daily time series for the same year (see Lorenz and Hartmann 2006). A Lanczos low-pass time filter (Duchon 1979) is then applied to exclude synoptic-scale activities with periods of less than 8 days. The latter step eliminates the contributions of tropical storms and easterly waves to the time series being analyzed. The results reported in the following sections are based on the filtered time series extending from 21 June to 31 August of each year.

## 3. Evolution of atmospheric features associated with ISV of NAM rainfall

### *a. NAM rainfall index*

Figure 1a shows the climatological summer (June–August) mean rainfall over the NAM region based on the NARR data. The heaviest summer monsoon rainfall occurs over the coastal region of northwestern Mexico along the western slope of the Sierra Madre (SM) Occidental. The rainfall over this region is characterized by vigorous diurnal convection activities, with peaks in late afternoon/early evening due to orography lifting of land–sea breeze and mountain/valley circulations (Negri et al. 1994; Berbery 2001; Tian et al. 2005). The NAM rainfall extends northward along the SM Occidental to the southwestern United States, in particular Arizona and western New Mexico. Note that an artificial gap in the rainfall pattern is apparent along the United States–Mexico border in the NARR due mainly to the lack of gauge observations in that region, as the rainfall field in the NARR largely relies on gauge observations over land. The counterpart of Fig. 1a, as constructed using data from the Global Precipitation Climatology Project (GPCP; Huffman et al. 2001) for the 1997–2004 period, is presented in Fig. 1b. There is a strong resemblance between the NARR and GPCP climatologies. In view of the higher spatial resolution in the NARR data, as well as the stronger dynamical consistency between rainfall and various circulation fields in this product, we proceed to construct an index of the NAM by using the NARR rainfall data. In view of the density of gauge observations in the NAM region, one would expect that NARR rainfall data are more accurate in the United States than in Mexico. Thus, the area over Arizona and New Mexico (AZNM hereafter) between 32°–36°N and 112–107°W (see purple rectangular box in Fig. 1a) is chosen for computation of the areal average rainfall index. The selection of this domain is nearly identical to that adopted in previous studies (e.g., Higgins et al. 2004; Kiladis and Hall-McKim 2004).

In Fig. 1c, the climatological daily evolution of rainfall over AZNM based on the NARR is shown. The monsoonal nature of the seasonal rainfall evolution is apparent: dry conditions prevail in June, whereas the rainfall amount dramatically increases in a very abrupt fashion in early July. The heavy rainfall continues during the summer season through the middle of September, and decreases thereafter. Higgins et al. (1997) have reported 7 July as the climatologically averaged onset date of the monsoon over AZNM. Their finding is consistent with the time series in Fig. 1c.

In the following presentation, we mainly use lag-regression patterns versus the standardized AZNM rainfall index (as computed using 8-day low-pass-filtered precipitation data) to describe the evolution of various atmospheric features associated with changes in the NAM intensity. The regression coefficients plotted in these charts represent the anomaly amplitudes corresponding to a change in the AZNM index of one standard deviation. A similar approach has been adopted in the studies of Kiladis and Hall-McKim (2004) and Lorenz and Hartmann (2006). Composite analyses based on strong rainfall events over AZNM (figures not shown) produce similar results. The statistical significance of the regression coefficients is as-

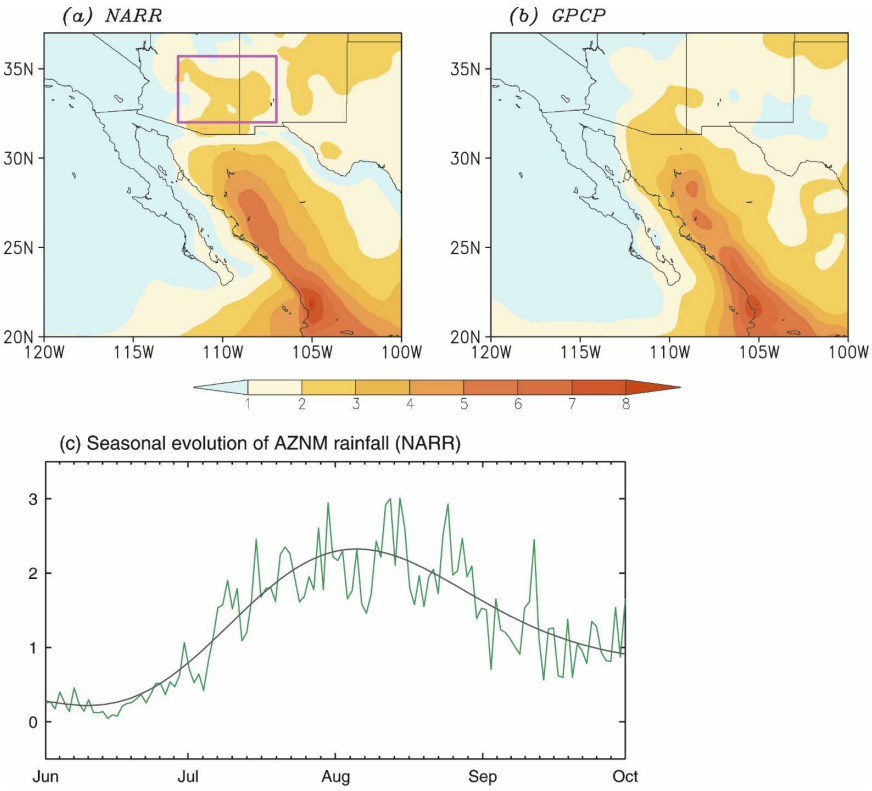


FIG. 1. Distributions of climatological summer precipitation over the NAM region, based on (a) NARR and (b) GPCP data (see color scale; units: mm day$^{-1}$). (c) Daily time series of climatological rainfall over Arizona and western Mexico [see purple rectangle in (a)] based on NARR data during 1979–2001 (green curve; units: mm day$^{-1}$). A smoothed climatological seasonal cycle of rainfall is also depicted by the black curve, which retains the time mean and first six harmonics of the annual cycle, as determined on the basis of 23-yr averages.

sessed by testing the null hypothesis that the associated correlation coefficients are different from zero, through application of a two-sided Student's $t$ test. Since time filtering has been applied to various datasets, the number of degrees of freedom (DOF) is greatly reduced as compared to the original sample size (about 1600 daily values). The effective DOF for each variable at each grid point over the Northern Hemisphere between the equator and 70°N has been estimated following Livezey and Chen (1983), and is found to be about one-fourth of the original sample size.

### b. *Local features associated with ISV of NAM*

Figure 2 shows the regression charts of rainfall at individual grid points versus the daily AZNM rainfall index at various lags. The interval between the time lags used in constructing the successive panels in this figure is 2 days. Only those rainfall signals surpassing the 95% significance level are shown. The results illustrate that the rainfall center over AZNM at day 0 can be traced back to the rainfall over the Gulf of Mexico (GoM) and tropical eastern Pacific more than one week earlier. On day −10, the heaviest rainfall is located over coastal regions of Mexico, with one center in the western GoM and another over the eastern edge of the tropical Pacific. Regression charts of the height field (to be shown later) suggest that this rainfall pattern is related to a large-scale circulation system at lower levels, and might result from the interaction of this atmospheric system with the complex terrain over Mexico (e.g., the SM Occidental and Oriental). In the ensuing days (day −8 to day −4), wet conditions still prevail over eastern Mexico, whereas enhanced rainfall spread northwestward along the slope of SM Occidental. On day −4, the rainfall maximum along the SM Occidental arrives at northwestern Mexico, just to the south of Arizona. Thereafter, the rainfall center migrates farther northward into the AZNM region. After it arrives at AZNM on day 0, the rainfall decreases markedly and eventually dissipates over the southwestern United States on day 4. It is interesting to note that a negative

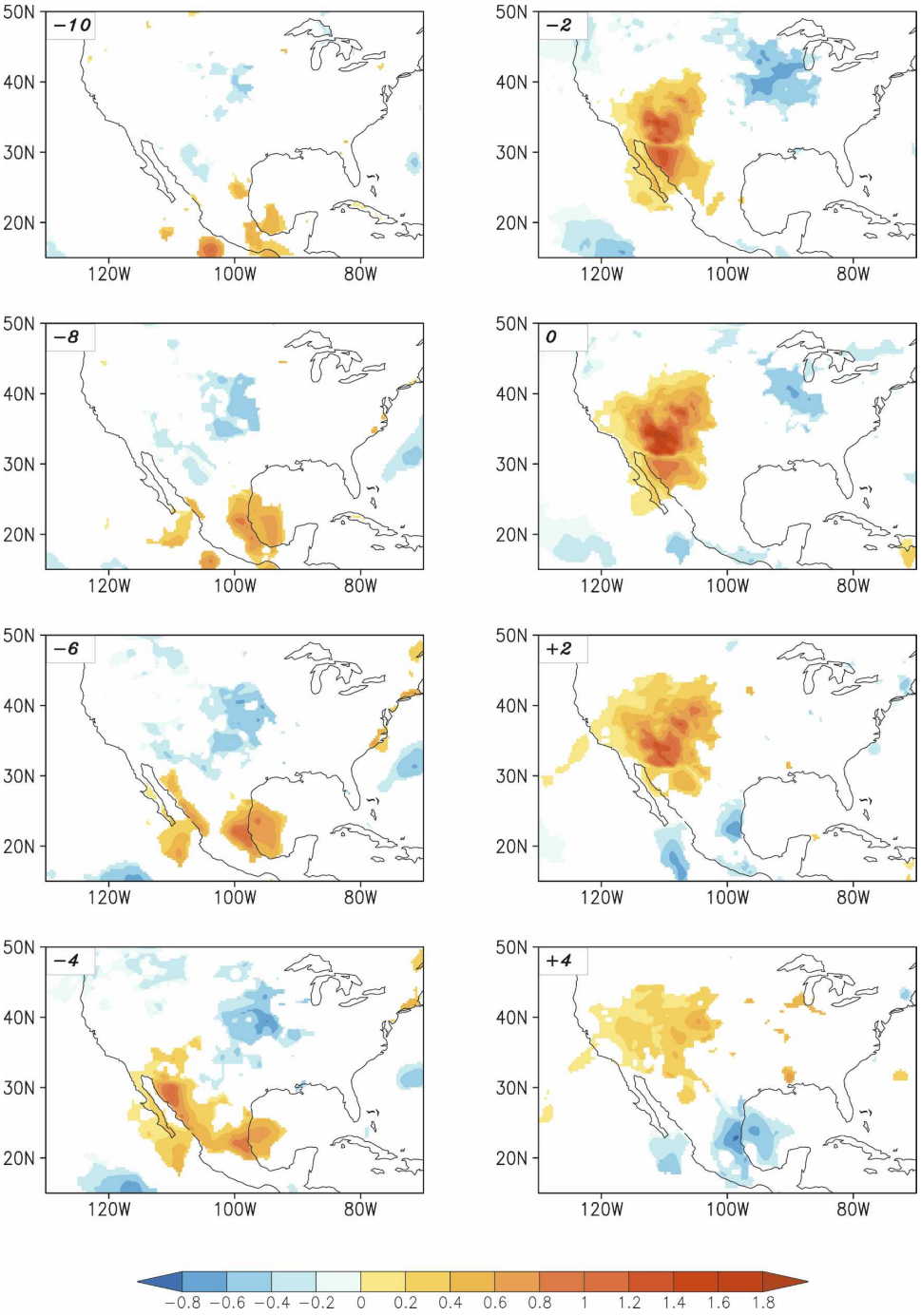


FIG. 2. Distributions of regression coefficients of 8-day low-pass-filtered rainfall vs the standardized AZNM rainfall index at time lags ranging from day −10 to day +4, as computed for the NAM season (21 Jun–31 Aug) during the 1979–2001 period. Only regression coefficients surpassing the 95% significance level are plotted (units: mm day$^{-1}$).

rainfall anomaly emerges over coastal Mexico along 20°N on day 2. Comparison among the individual panels in Fig. 2 indicates that the rainfall pattern on day 4 and that on days −8 or −6 represent two opposite phases of the rainfall evolution, thus suggesting that the rainfall variation over the NAM region has a cyclical character, with an intraseasonal time scale of about 20 days. This result is in agreement with previous studies on the dominant period of NAM variability (e.g., Mullen et al. 1998; Mo 2000).

It is also noteworthy that the enhancement of rainfall over the NAM region is accompanied by a deficient rainfall pattern over the U.S. Great Plains. As discussed in the introduction, the out-of-phase relationship between the rainfall over the southwestern United States and Great Plains has been documented in previous studies, and is discernible on a broad range of time scales, including interannual variability (Higgins et al. 1999) and seasonal cycle (Higgins et al. 1997). In the present study, we shall focus on the large-scale circulation associated with this dipolelike rainfall pattern on intraseasonal time scales.

To gain a better understanding of the evolution of rainfall features described above, the regional-scale circulation pattern over North America associated with rainfall variability over AZNM is further analyzed using regression maps of geopotential height and wind vectors at different vertical levels and at time lags ranging from day −8 to day 2. In Fig. 3, these charts for 200, 500, and 850 hPa are displayed in the left, middle, and right columns, respectively, and the results for individual lags are arranged vertically within each column. Note that the scales for color shading and wind vectors are different for each pressure level, as indicated at the bottom of the columns.

At 200 hPa (left column), about one week prior to the rainfall peak over AZNM (day −8 to day −6), an anticyclonic circulation center appears over the western United States at 40°N. This feature remains quasi-stationary between day −6 and day −2. At the same time, an intensifying cyclonic vortex travels westward over the GoM. After day −2, as the rainfall over AZNM attains maximum intensity, the anticyclonic center over the western United States starts to move eastward. The subtropical cyclonic vortex over the GoM quickly extends westward from day −2 to day 0. Thereafter, this feature gains further strength as it propagates northwestward over the Pacific Ocean off Baja California.

Inspection of the circulation patterns at 500 and 850 hPa illustrates that the midlatitude high over the United States exhibits an almost equivalent barotropic structure, with a slight westward tilt with increasing height in the lower troposphere. (The circulation patterns at 700 hPa largely resemble those at 500 hPa, and thus are not shown here.) The subtropical cyclone feature, however, displays a complicated vertical structure. While the westward movement of the low center from Florida to Mexico is evident at 200 hPa, the low center at 500 hPa is mainly situated over western Mexico/the eastern Pacific. At 850 hPa, the negative height perturbations in the subtropics are mainly confined above the ocean surface of the eastern Pacific and western GoM. From day −8 to day −2, the low center over western GoM gradually diminishes. After day −2, the vortex over the eastern Pacific undergoes northwestward movement along the coastal region off California as detected at other vertical levels. The behavior of the low-level wind and height pattern is consistent with the rainfall evolution features shown in Fig. 2, suggesting that the low-level circulation may play a pivotal role in modulating the rainfall evolution over ANZM.

Particularly noteworthy is the prevalence of southeasterly flow at 850 hPa along GoC on day 0, when maximum rainfall occurs over AZNM. This low-level wind anomaly is associated with the cyclonic circulation over the eastern Pacific and anticyclonic circulation over the continental United States, and markedly resembles the synoptic situation during typical gulf surge events, as depicted in many previous studies (e.g., Stensrud et al. 1997; Bordoni and Stevens 2006). The same characteristic low-level circulation pattern at day 0 is reminiscent of the setting favoring the "wet surge" events over the southwestern United States, as illustrated by Higgins et al. (2004, their Fig. 13). The important role of the southeasterly low-level flow in modulating NAM rainfall on interannual time scales has also been noted by Carleton et al. (1990). Furthermore, the evolution of rainfall and circulation features associated with rainfall variations over ANZM is in broad agreement with the results of Kiladis and Hall-McKim (2004).

To delineate the moisture transport contributing to the rainfall over AZNM, we proceed to examine the regression charts for vertically integrated moisture, moisture flux, and its divergence over that region. The results, as obtained for the atmospheric column extending from the surface to 100 hPa at day 0, are shown in Fig. 4. In accord with the occurrence of heavy rainfall over AZNM at this time (Fig. 2), a maximum center of specific humidity appears near the northern tip of GoC in the moisture pattern (Fig. 4a). A negative moisture anomaly is evident near the Great Lakes, where the rainfall is reduced at this time. The enhanced (decreased) moisture content over the southwestern (northern central) United States is accompanied by vertically integrated moisture convergence (divergence), as illustrated by shading in Fig. 4b. The moisture flux vectors further suggest that the moisture convergence over the southwestern United States may largely be attributed to moisture transport from the Pacific Ocean by southerly flow on the eastern flank of the anomalous cyclonic circulation. On the other hand, the moisture divergence south of the Great Lakes is mainly associated with the anticyclonic circulation over the continental United States. Further analysis indicates that the

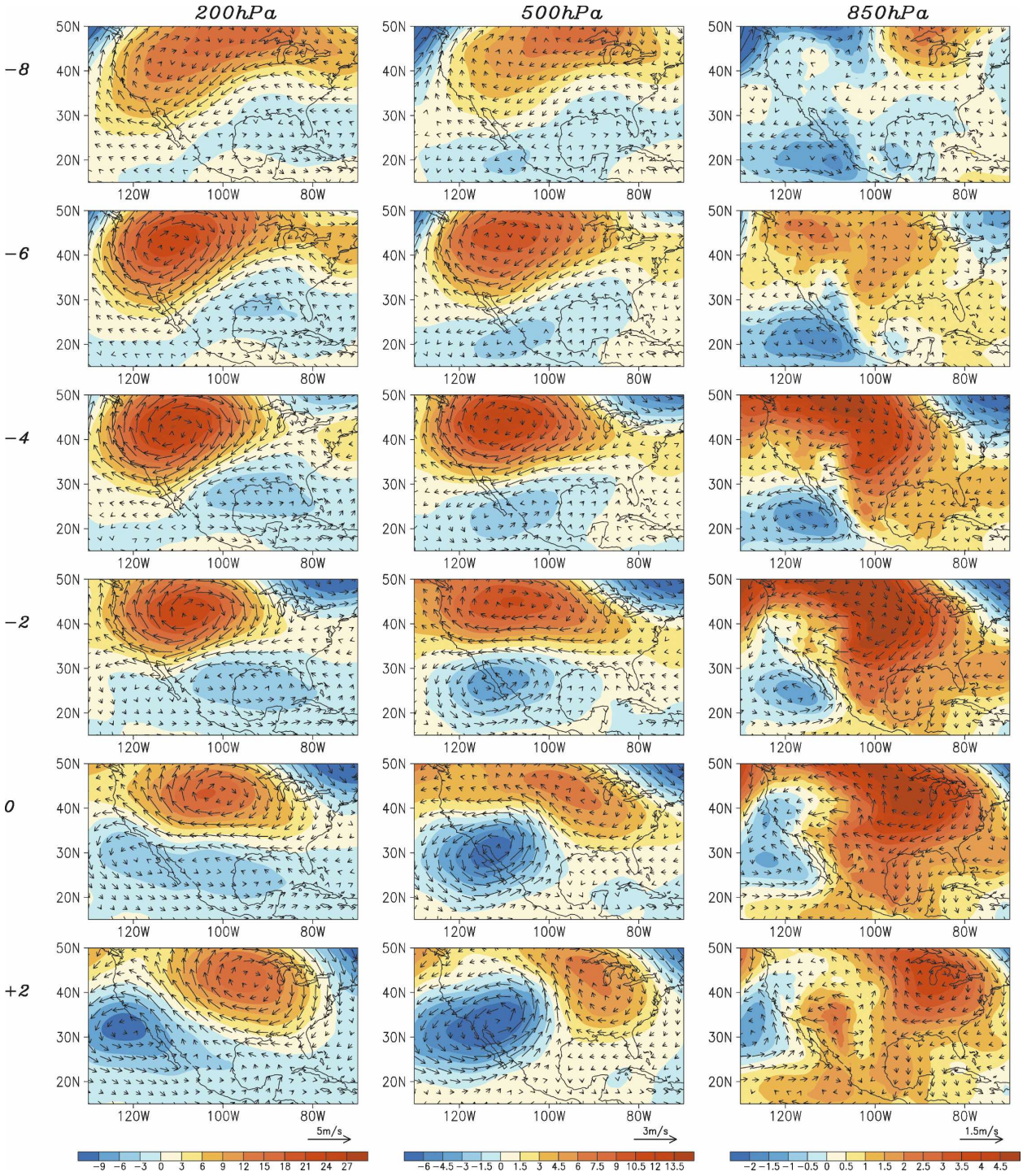


FIG. 3. Distributions of the regression coefficients of the 8-day low-pass-filtered geopotential height (shading) and wind vectors (arrows) vs the standardized AZNM rainfall index at time lags ranging from day −8 to day 2, for the (left) 200-, (middle) 500-, and (right) 850-hPa levels. The scales for the geopotential height (units: m) and wind vectors for each pressure level are indicated at the bottom of the respective column. All computations are based on NARR data.

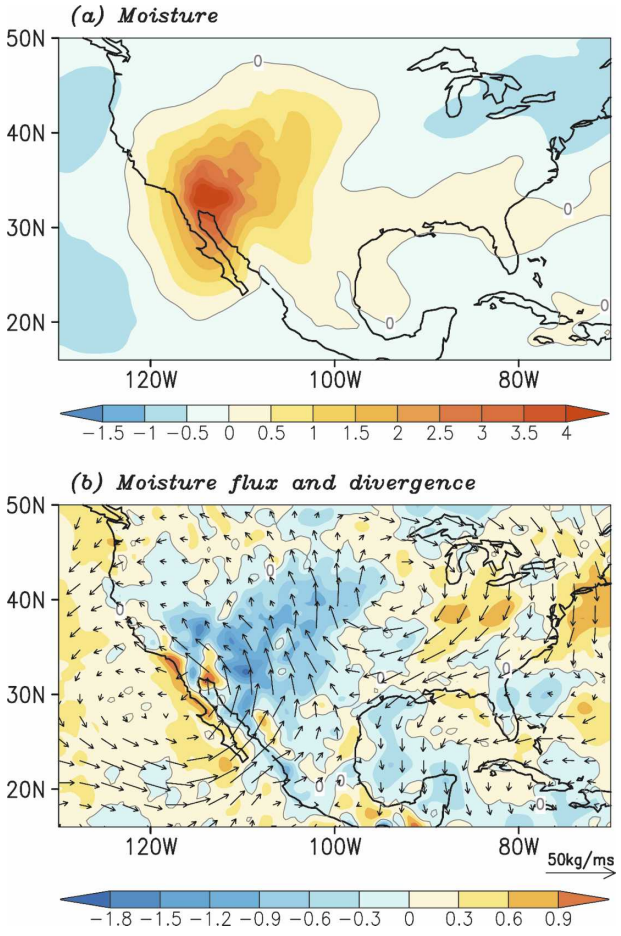


FIG. 4. Distributions of the regression coefficients of vertically integrated 8-day low-pass-filtered (a) specific humidity (units: g $kg^{-1}$) and (b) moisture flux (arrows; see scale at upper right) and moisture flux divergence (shading; units: mm $day^{-1}$) vs the standardized AZNM rainfall index at zero time lag. All computations are based on NARR data.

vertically integrated moisture and moisture flux receive the largest contributions from changes within the layer between the surface and 700 hPa.

The above results suggest that the low-level circulation pattern, with a low vortex over the subtropical eastern Pacific, a midlatitude high anomaly over the central United States, and prevailing southeasterly winds along the GoC, may play an essential role in modulating the NAM rainfall. In the next section, we proceed to link these regional features with global-scale teleconnection patterns.

## 4. Global teleconnections

### *a. Geopotential height and OLR patterns*

Figure 5 shows regression patterns of 200-hPa geopotential height and wind fields versus the standardized AZNM rainfall index. These charts are analogous to those presented in the left column of Fig. 3, except that they are based on ERA-40 data with global coverage. The features in the North American sector, as noted in the left column of Fig. 3, are also evident in Fig. 5. The patterns in the expanded domain used for plotting Fig. 5 reveal that the regional-scale circulation anomalies over North America are linked with a global wave train. The establishment of the anticyclonic anomaly over the western United States on day −6 is seen to be accompanied by a strong cyclonic center over the eastern North Pacific, as previously pointed out by Kiladis and Hall-McKim (2004). The origins of the wave train connecting these centers in the North Pacific–western United States can be traced all the way back to the western Pacific and Eurasia. This wave train appears to consist of two branches. The first branch links the disturbances over the Mediterranean to those over North America via East Asia, with individual centers being aligned with the summertime midlatitude westerly jet (as will be illustrated in the next subsection). This summertime wave train over the Eurasian continent is often referred as the "silk road" teleconnection pattern by many studies (e.g., Enomoto et al. 2003; Ding and Wang 2005). The other branch of the wave train connects the wave disturbances over the subtropical western North Pacific with those over the North Pacific/North America, and acquires an arch shape that follows a "great circle" route. These two branches merge with each other over the region between Japan and the date line. The evolution of the patterns in Fig. 5 indicates westward phase propagation of the individual centers over the North Pacific, particularly during the period from day −6 to day 0.

The corresponding evolution of the global circulation at 850 hPa associated with ISV of the NAM rainfall is presented in Fig. 6. While the silk road teleconnection pattern becomes rather weak at this level, the arch-shaped trans-Pacific wave train connecting circulation centers over the WNP with those over the eastern subtropical Pacific/North America is more evident in the lower troposphere than at 200 hPa. A Monte Carlo field significance test following Livezey and Chen (1983) shows that these wave train patterns at 850 hPa from day −4 to day 0 are significant at the 90%–95% level. Westward migration of the centers over the Pacific along this wave train is again clearly discernible at 850 hPa. The low-level cyclonic center over the eastern Pacific Ocean near 120°W, which plays an essential role in modulating rainfall variation over the NAM region as previously noted, is apparently one component of this trans-Pacific wave train. Moreover, the northwestward movement of this vortex over the eastern Pacific

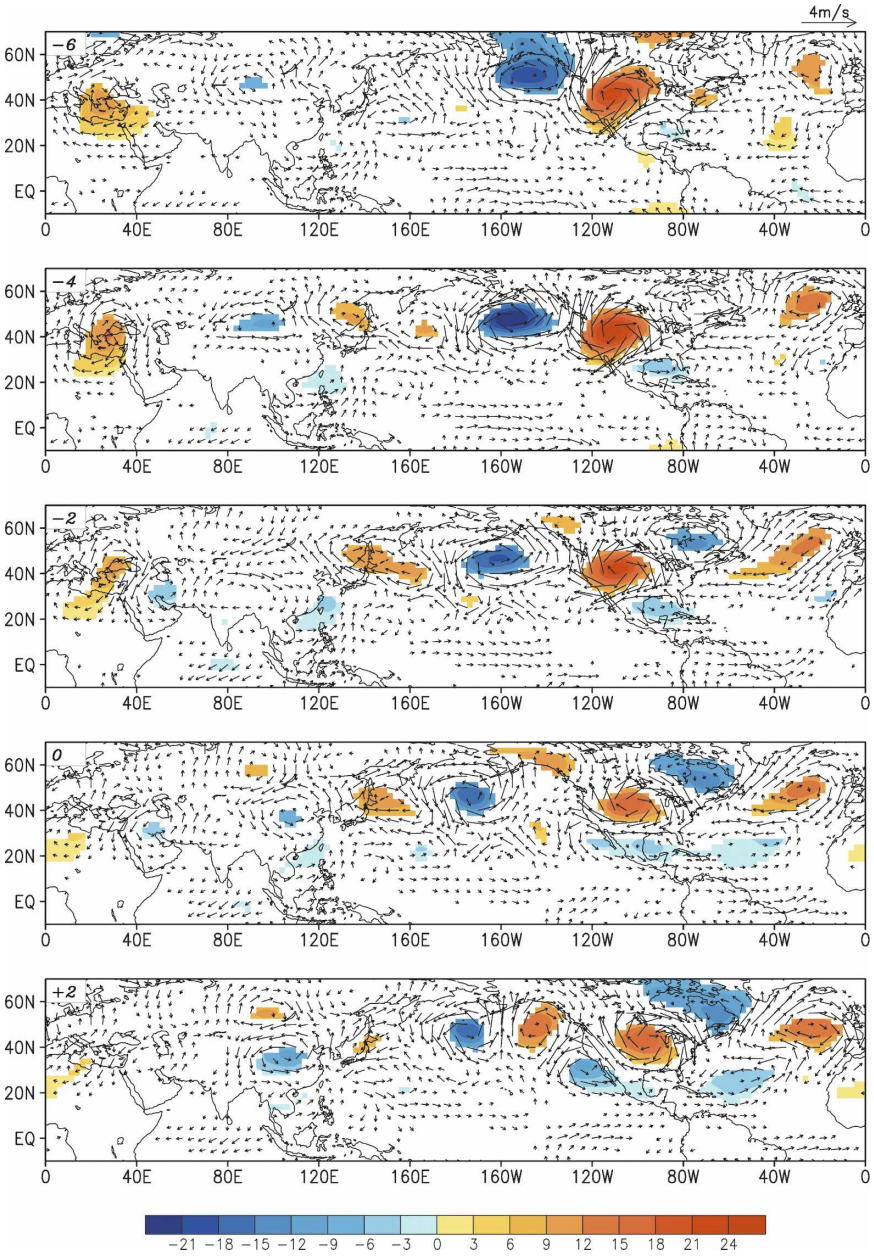


FIG. 5. Distributions of regression coefficients of 8-day low-pass-filtered 200-hPa geopotential height (shading; units: m) and wind vectors (arrows; see scale at upper right) vs the standardized AZNM rainfall index at time lags ranging from day −6 to day 2. Only geopotential signals surpassing the 90% significance level are plotted. Wind vectors smaller than 0.25 m $s^{-1}$ are omitted. The height and wind data are obtained from ERA-40.

off California is associated with the overall counterclockwise propagation of the individual centers along the entire length of the wave train spanning over the North Pacific. On day −6, a prominent anticyclonic center is located over the Philippine and South China Seas (i.e., in the westernmost part of the trans-Pacific wave train). In conjunction with the overall counterclockwise propagation of the perturbations embedded in this wave train, this anticyclonic center moves southwestward to the South China Sea and the Indo-China Peninsula.

Comparison between Figs. 5, 6 indicates that the circulation features along the North Pacific segment of the wave train exhibit an almost equivalent barotropic

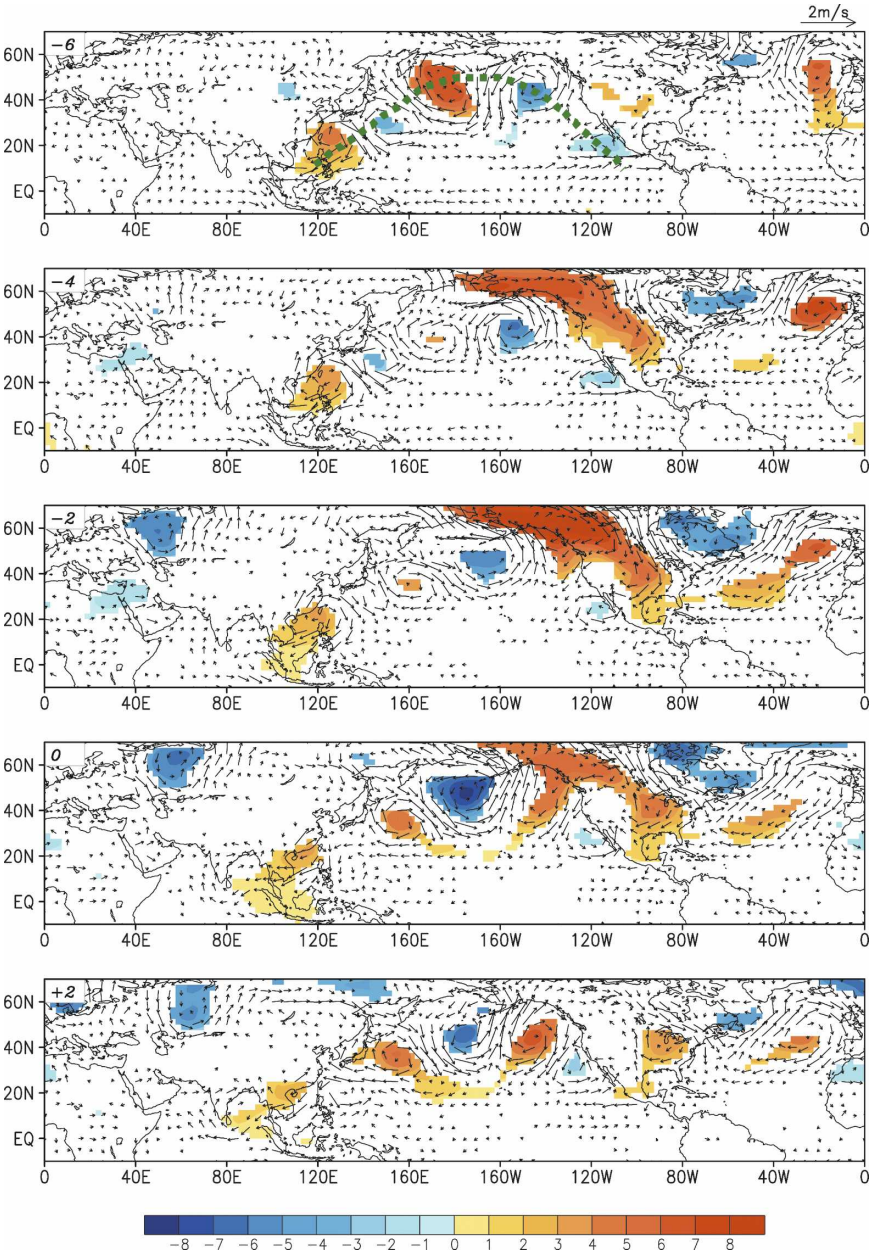


FIG. 6. Same as Fig. 5, but for 850 hPa. The green dashed line in the top panel indicates the axis of the trans-Pacific wave train.

structure. In contrast, the anomalies have a distinct baroclinic character near the Philippine Sea, with a high center at low level being overlain by a low center at upper level. Such differences in the vertical structure in various portions of the wave train are clearly evident in Fig. 7, which shows the cross section of geopotential height perturbations along the wave train axis on day −6 (see green dashed line in the upper panel of Fig. 6). A predominantly barotropic structure prevails at most locations, except those over the WNP near 120°E. The baroclinic character over the WNP is suggestive of the important role of latent heat release associated with convection in that region; whereas the equivalent barotropic structure in the remaining portion of the wave train is the signature of Rossby wave energy dispersion. In view of the placement of the baroclinic structure near the western edge of the wave train, this wave train is likely a response to the convective activity over the WNP.

Global lag-regression patterns have also been constructed using the OLR dataset, in order to highlight

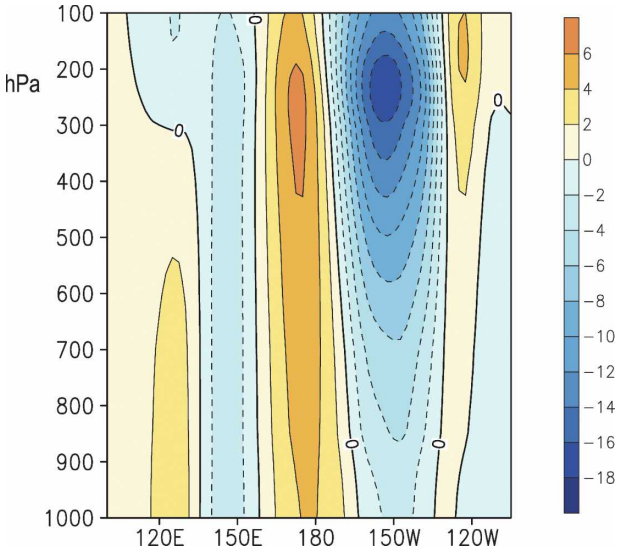


FIG. 7. Vertical cross section of the regression coefficients of 8-day low-pass-filtered geopotential height vs the standardized AZNM rainfall index at the time lag of day −6 (units: m). The abscissa corresponds to the axis of the Pacific wave train, as denoted by the green dashed line in the top panel of Fig. 6. The height data are obtained from ERA-40.

the convection activities in various regions that are associated with ISV of the NAM rainfall. The results are displayed in Fig. 8. (Note that negative anomalies of the OLR represent the enhanced convection, and vice versa.) The OLR signals over the NAM region in Fig. 8 are consistent with the precipitation charts in Fig. 2 based on the NARR. A strong convective center first appears over the coastal region of Mexico (day −6), and then migrates northwestward along the slope of SM Occidental to the southwestern United States. Furthermore, the patterns in Fig. 8 reveal that the trans-Pacific wave train, as previously identified using geopotential height data, is also associated with distinct perturbations in convective activity. The alternate high (low) centers along the wave train at 850 hPa (Fig. 6) are generally collocated with suppressed (enhanced) convection, especially over the tropical and subtropical regions. In particular, convection is suppressed over the high anomaly in the WNP associated with ISV of NAM rainfall. The center of this positive geopotential height perturbation at 850 hPa is displaced northwestward of the center of suppressed convection (cf. Figs. 6, 8). This spatial relationship has also been noted by Hsu (2005) for the circulation pattern associated with the summertime intraseasonal convective activity over the WNP, and is consistent with the atmospheric Rossby wave response to the diabatic heating as proposed by Gill (1980). The center of suppressed convection over the WNP also moves southwestward with time, following the path taken by the high anomaly in that region (see Fig. 6).

The above results indicate that the low-level circulation changes over the WNP could be a response to the suppressed convection over that region. Since the WNP is located on the upstream side of the trans-Pacific wave train, the convective activity therein might play an essential role in modulating the rainfall variability of the NAM through perturbing the disturbances along that wave train. As a further test of this hypothesis, similar regression patterns of the geopotential height and wind vectors at 850 hPa against OLR over the WNP (10–25°N, 120–140°E) have been calculated based on 8-day low-pass-filtered data. The regression pattern on day 0 is displayed in Fig. 9. The most prominent feature in this figure is the trans-Pacific wave train extending from the WNP to the tropical eastern Pacific. This feature is very similar to that illustrated in previous regression patterns based on the NAM rainfall index (Fig. 6). The westward propagation of the wave train is also discernible in the regression maps at different time lags (figures not shown). This result further substantiates the important role of convective activity over the WNP in generating the trans-Pacific wave train.

### b. *Wave-activity flux*

The nature of energy propagation along the wave train described in the previous subsection may be further diagnosed using the wave-activity flux vector (Takaya and Nakamura 2001; Tam and Lau 2005). Only the horizontal components of the activity vector **W** are considered here:

$$\mathbf{W} = \frac{1}{2|\mathbf{U}|}\begin{bmatrix} U(\psi_x^2 - \psi\psi_{xx}) + V(\psi_x\psi_y - \psi\psi_{xy}) \\ U(\psi_x\psi_y - \psi\psi_{xy}) + V(\psi_y^2 - \psi\psi_{yy}) \end{bmatrix},$$

where $\psi$ is the perturbation streamfunction, the subscripts represent partial derivatives, and $\mathbf{U} = (U, V)$ is the two-dimensional time mean flow. Convergence of the activity flux leads to amplification of the wave pseudomomentum, which is a measure of a combination of the wave energy and enstrophy. It can be shown that the wave-activity vector is parallel to the group velocity of Rossby waves in the plane wave limit. The calculation of this activity flux does not depend on any spatial or time averaging, making it ideal for depicting the three-dimensional pattern of wave activity at any particular time (see Takaya and Nakamura 2001 for details).

Figure 10 shows the regression patterns for wave-activity flux (vectors) and its divergence (shading) at 200 and 850 hPa on day −6, when an anticyclonic anomaly starts to develop over the western United

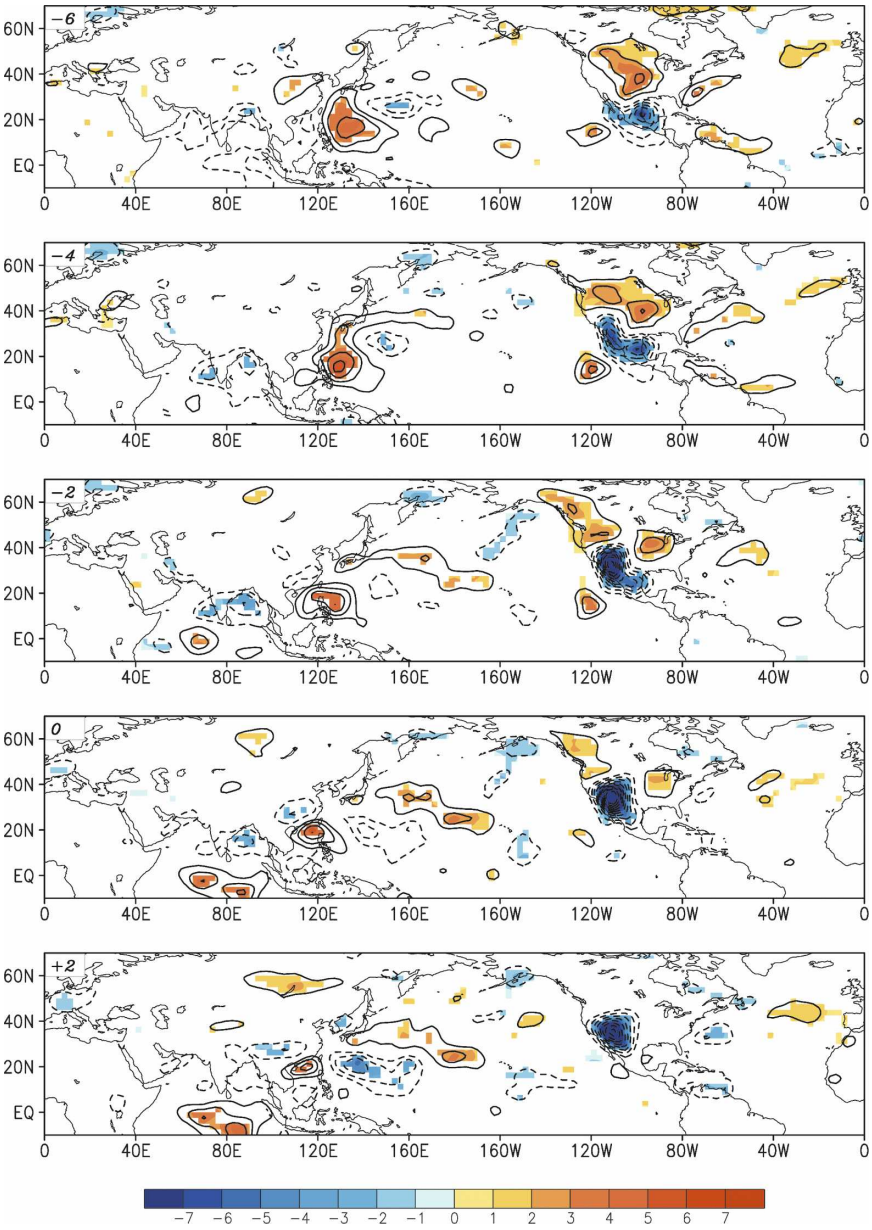


FIG. 8. Distributions of regression coefficients of 8-day low-pass-filtered OLR vs the standardized AZNM rainfall index at time lags ranging from day −6 to day 2 (contours and color shading). Contour interval: 1 W $m^{-2}$ (solid and dashed contours indicate positive and negative values, respectively; zero contours are not shown). Regression coefficients surpassing the 90% significance level are indicated by color shading (see scale bar at bottom; units: W $m^{-2}$).

States (see Fig. 3). The summer mean zonal wind at each level is also depicted using contours (only those indicating mean westerlies are plotted). It is seen that the establishment of the anticyclone over the western United States coincides with strong activity flux convergence at 200 hPa (Fig. 10a). The pattern for wave-activity flux suggests that the inflow of wave energy to this region mainly originates from the North Pacific near 160°E, where divergence of wave-activity flux is prevalent. Over the Eurasian continent, the wave-activity fluxes associated with the aforementioned silk road wave train pattern are directed from the Mediterranean region to Japan along the axis of the summertime jet stream (see contours). The weak wave-activity fluxes between Japan and 160°E at 40°N suggest that the energy flow from the Eurasian continent may not play an essential role in sustaining the North Pacific wave train. The general consistency between latitudes

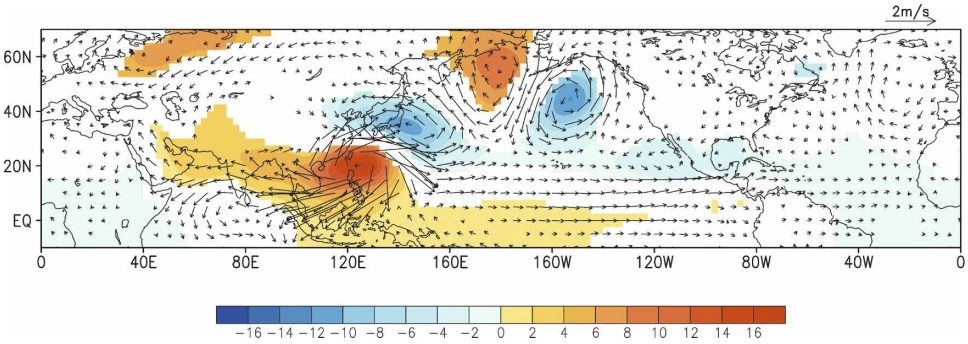


FIG. 9. Distributions of regression coefficients of 8-day low-pass-filtered 850-hPa geopotential height (shading; units: m) and wind vectors (arrows; see scale at upper right) vs the standardized OLR index over the WNP (10°–25°N, 120°–140°E) at zero time lag. Only geopotential signals surpassing the 95% significance level are plotted. Wind vectors smaller than 0.2 m $s^{-1}$ are omitted. The height and wind data are obtained from ERA-40.

of maximum wave activity and the summer mean westerly jet at 200 hPa confirms the important role of the midlatitude jet stream as a waveguide in organizing the wave disturbances (Hoskins and Ambrizzi 1993).

In the lower troposphere (Fig. 10b), the pattern of wave-activity flux indicates energy transport from the WNP to North America along the wave train axis (cf. Fig. 6). The energy source that maintains the low-level wave train is located over the WNP monsoon region near the Philippine Sea, where divergence of wave-activity flux occurs. Positive anomalies in geopotential height (Fig. 6) and OLR (Fig. 8) prevail over this region on day −6. Thus, the results in Fig. 10b provide further evidence on the key role of convective activities over the WNP monsoon region in generating and sustaining the trans-Pacific wave train. It is also worth noting that the arch-shaped pattern of the wave-activity fluxes over the North Pacific is collocated with strong mean westerlies associated with the climatological subtropical high residing over the western Pacific in the lower troposphere. This mean circulation may serve as a waveguide for the Rossby wave train.

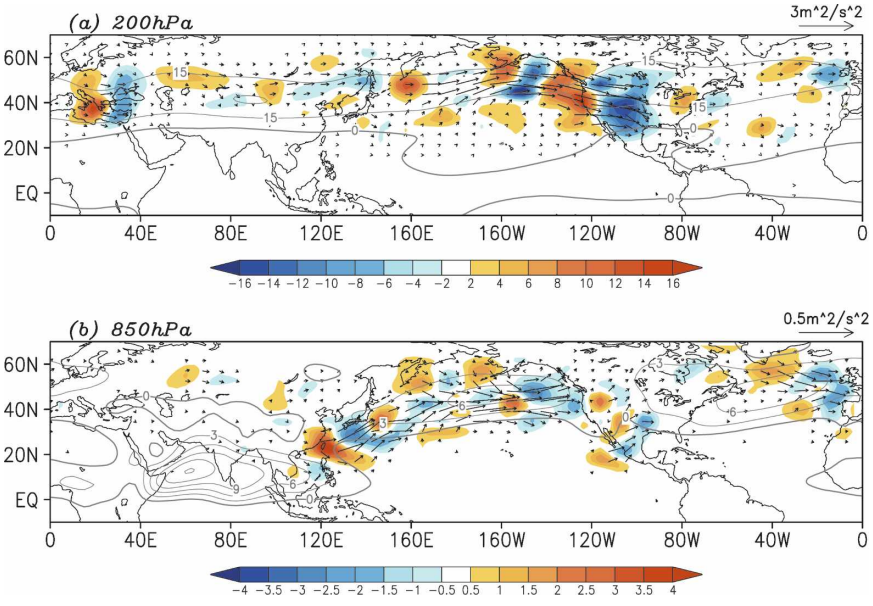


FIG. 10. Distributions of the regression coefficients of 8-day low-pass-filtered wave-activity flux (arrows; see scale at upper right) and wave-activity flux divergence (shading; units: m $s^{-2}$) vs the standardized AZNM rainfall index at time lag of day −6, and summer mean zonal wind component (contours; units: m $s^{-1}$; only positive values indicating westerlies are plotted), for (a) 200 and (b) 850 hPa. Data for the wave-activity flux and zonal wind are obtained from ERA-40.

The wave-activity flux patterns at other time lags versus the AZNM rainfall index (figures not shown) are similar to those displayed in Fig. 10, except that the amplitude of the fluxes over the Pacific weakens slightly after day −6, and the wave flux divergence pattern shifts slowly with time in conjunction with the migration of the convection centers over the subtropical NWP.

The above global teleconnection patterns associated with ISV of NAM rainfall are based on ERA-40. Very similar results are obtained by processing the NCEP–National Center for Atmospheric Research (NCAR) reanalysis dataset. The anomalous circulation patterns over North America associated with ISV of NAM rainfall, as reported in present study, are in good agreement with those obtained by Kiladis and Hall-McKim (2004) using NCEP–NCAR reanalyses. In that study, the authors have noted that NAM variability is associated with a similar wave train pattern at 500 hPa over the North Pacific. The inferences from their analysis of the E-vector pattern at 200 hPa over the North Pacific are similar to those based on the wave-activity fluxes examined in the present study. However, Kiladis and Hall-McKim (2004) only considered the circulation patterns in the mid- and upper troposphere, where the linkage between the WNP and North America through the trans-Pacific wave train is less evident than that at the lower levels.

## 5. Summary and discussion

In this study, the ISV of NAM with a time scale of about 20 days, as detected in previous studies (e.g., Mullen et al. 1998; Mo 2000; Kiladis and Hall-McKim 2004), has been confirmed based on the recently released NARR dataset. The rainfall signal of this intraseasonal mode first emerges near the GoM and eastern Pacific at 20°N about one week prior to the rainfall peak over the southwestern United States. Subsequently, the precipitation center over western Mexico migrates northwestward along the slope of the SM Occidental. This center rapidly dissipates after it arrives at AZNM. The most prominent local circulation features in the lower troposphere associated with enhanced rainfall over AZNM include a subtropical eastern Pacific cyclonic anomaly off the California coast, a midlatitude high anomaly over the western United States, and prevailing southeasterly winds along the GoC between the subtropical low and midlatitude high. This low-level southeasterly flow over the GoC bears strong resemblance to the wind pattern accompanying the "gulf surge" events as discussed in many previous studies. Such events play an active role in modulating the NAM rainfall by transporting moist marine air from oceanic areas to the southwestern United States, thus feeding the convection over that region. The low-level circulation over North America associated with the enhanced rainfall over AZNM is also in broad agreement with the flow pattern favoring "wet surge" events over the southwestern United States, as identified by Higgins et al. (2004).

We have further illustrated that ISV of the NAM rainfall is linked to convective activities over the WNP through a distinct trans-Pacific wave train that follows a "great circle" route. It is noted that the aforementioned low-level circulation pattern over North America associated with NAM rainfall variability is part of this trans-Pacific wave train. Further analysis illustrates that the geopotential height perturbations along the wave train exhibit an equivalent barotropic vertical structure over most locations except WNP, where a baroclinic structure prevails. The wave disturbances at upper (lower) level over the North Pacific along the wave train are mainly guided by the summer mean midlatitude (subtropical) westerly jet. These results are indicative of the importance of Rossby wave energy dispersion in maintaining this trans-Pacific wave train (Hoskins and Ambrizzi 1993). Further analysis based on a global OLR dataset confirms that the lower- (upper) level anticyclonic (cyclonic) circulation over the WNP is associated with a distinct center of suppressed convection. The circulation features are displaced northwestward of the OLR anomaly, thus suggesting that they are Rossby wave responses to perturbed diabatic heating, as proposed by Gill (1980). The convection-driven disturbances over the WNP are situated upstream of the Pacific wave train, and may serve as an energy source for generating and maintaining the wave train. This hypothesis is supported by a very similar trans-Pacific wave train appearing in the regression patterns of geopotential height and winds at 850 hPa against OLR over the WNP. Furthermore, a wave activity diagnosis also clearly indicates pronounced energy emanation from subtropical WNP to North America in the lower troposphere following the great circle path. In the upper troposphere, the analysis indicates that the energy source for the wave train over the North Pacific is located east of Japan along the jet stream, where the upper-level wave train merges with its lower-level counterpart. This result suggests that the impact of the convective heating over the WNP on the North American climate may be realized through the heating-induced meridional circulation that disturbs midlatitude jet stream.

The individual circulation centers within the trans-Pacific wave train exhibit slow counterclockwise migration along the great circle path. As part of this evolution, the low-level subtropical cyclonic gyre over the

eastern Pacific moves northwestward along the U.S. California coast, in concert with the northwestward migration of the rainfall center along the slope of the SM Occidental. By the same token, the low-level anticyclonic anomaly over the WNP moves southwestward to the South China Sea and Indochina Peninsula.

Most of the aforementioned large-scale circulation features associated with ISV of rainfall over the NAM region are discernible in regression patterns of unfiltered large-scale variables against the NAM rainfall index (figures not shown). The consistency between results based on filtered and unfiltered data further affirms the robustness of the findings presented in this study.

It is worth noting that the ISV with a time scale of about 20 days associated with the East Asian (EA)/WNP monsoon has also been documented in many previous studies (see Hsu 2005 for a review). Of particular interest are the investigations of Fukutomi and Yasunari (1999, 2002), who examined the spatial and temporal evolution of the 10–25-day intraseasonal variations over the WNP during June–August by using the OLR over 10°–20°N and 100°–120°E as an index for composite analysis. Their results are very similar to those illustrated in the present study, including a distinct wave train extending from the WNP to the North Pacific, transition from a baroclinic structure over WNP to an equivalent barotropic structure farther downstream, and southwestward movement of the low-level circulation and convective center over WNP. Note that the 8-day low-pass-filtered AZNM rainfall index employed in the present study has not been subjected to time filtering with a specific intraseasonal time scale. Hence the agreement between the findings in our study and those in previous works on ISV in the Asian sector offers independent substantiation of the strong linkage between the WNP/EA monsoon and the NAM on intraseasonal time scales.

The salient features related to ISV of the NAM as revealed in the present study based on the NARR dataset are largely in accord with those noted by Kiladis and Hall-McKim (2004), who mainly examined the NCEP–NCAR reanalyses. It is particularly worth mentioning that in their study the variability of the NAM rainfall associated with the MJO has been removed by high-pass filtering the precipitation data with a 30-day cutoff prior to the regression analysis. Thus, the agreement between the results in the present study (which encompass all intraseaonal fluctuations with time scales longer than 8 days) and those in Kiladis and Hall-McKim (2004) implies that the eastward-propagating MJO along the equator (with typical periods longer than 30 days) may not be an essential contributor to ISV of the NAM rainfall as described in this article.

The summertime teleconnection between rainfall over the Asian/North Pacific monsoon region and North America via trans-Pacific wave trains has been reported for interannual time scales (Lau and Weng 2000, 2002; Wang et al. 2001; Z. Wang et al. 2007, personal communication) and for intraseasonal periods of 40–50 days (e.g., Kawamura et al. 1996). The characteristic wavelength of the disturbances along the wave trains associated with these longer time scales is typically longer than that for the 20-day fluctuations discussed in this study.

While we have provided evidence on the potential impacts of convective activities over the WNP on NAM with 20-day time scales, further investigations are warranted to study the physical mechanisms contributing to this teleconnection. For instance, the origins of ISV of the EA/WNP monsoon with 20-day periods are still not fully understood. Fukutomi and Yasunari (1999) suggested that ISV over the WNP on 10–20-day time scales results from the mutual interaction between the tropics and the extratropics. They argued that oscillations of convection over the WNP are initiated by the southwestward movement of circulation anomalies, which in turn trigger downstream developments along the Pacific wave train through Rossby wave energy dispersion. It is still not clear if this ISV with 20-day periods over the WNP is the result of local convection–thermal feedback (Gyoswami and Shukla 1984) or air–sea interaction (Wang and Zhang 2002; Lau and Nath 2006). Further study is also needed to delineate the physical processes contributing to the westward propagation of intraseasonal oscillations on 20-day time scales over the WNP.

*Acknowledgments.* We are grateful to I. Held, I. Orlanski, and G. Kiladis for constructive discussions in the course of this study. We would also like to thank G. Vecchi, J. Lanzante, G. Kiladas, Q. Ding, Z. Wang, and B. Wang and the anonymous official reviewers for their insightful comments, which led to considerable improvements of earlier versions of this manuscript. XJ acknowledges the support of the AOS visiting scientist program at Princeton University.

## REFERENCES

Adams, D. K., and A. C. Comrie, 1997: The North American monsoon. *Bull. Amer. Meteor. Soc.,* **78,** 2197–2213.

Berbery, E. H., 2001: Mesoscale moisture analysis of the North American monsoon. *J. Climate,* **14,** 121–137.

Bordoni, S., and B. Stevens, 2006: Principal component analysis of the summertime winds over the Gulf of California: A gulf surge index. *Mon. Wea. Rev.,* **134,** 3393–3412.

——, P. E. Ciesielski, R. H. Johnson, B. D. McNoldy, and B. Stevens, 2004: The low-level circulation of the North Ameri-

can Monsoon as revealed by QuikSCAT. *Geophys. Res. Lett.,* **31,** L10109, doi:10.1029/2004GL020009.

Carleton, A. M., D. A. Carpenter, and P. J. Weser, 1990: Mechanisms of interannual variability of the southwest United States summer rainfall maximum. *J. Climate,* **3,** 999–1015.

Ding, Q., and B. Wang, 2005: Circumglobal teleconnection in the Northern Hemisphere summer. *J. Climate,* **18,** 3483–3505.

Douglas, M. W., R. Maddox, K. Howard, and S. Reyes, 1993: The Mexican monsoon. *J. Climate,* **6,** 1665–1667.

Duchon, C. E., 1979: Lanczos filtering in one and two dimensions. *J. Appl. Meteor.,* **18,** 1016–1022.

Enomoto, T., B. J. Hoskins, and Y. Matsuda, 2003: The formation mechanism of the Bonin high in August. *Quart. J. Roy. Meteor. Soc.,* **129,** 157–178.

Fukutomi, Y., and T. Yasunari, 1999: 10–25 day intraseasonal variations of convection and circulation over East Asia and western North Pacific during early summer. *J. Meteor. Soc. Japan,* **77,** 753–769.

——, and ——, 2002: Tropical–extratropical interaction associated with the 10–25 day oscillation over the western Pacific during the northern summer. *J. Meteor. Soc. Japan,* **80,** 311–331.

Fuller, R. D., and D. J. Stensrud, 2000: The relationship between tropical easterly waves and surges over the Gulf of California during the North American monsoon. *Mon. Wea. Rev.,* **128,** 2983–2989.

Gill, A. E., 1980: Some simple solutions for heat-induced tropical circulation. *Quart. J. Roy. Meteor. Soc.,* **106,** 447–462.

Gyoswami, B. N., and J. Shukla, 1984: Quasi-periodic oscillations in a symmetric general circulation model. *J. Atmos. Sci.,* **41,** 20–37.

Hales, J. E., Jr., 1972: Surges of maritime tropical air northward over the Gulf of California. *Mon. Wea. Rev.,* **100,** 298–306.

Higgins, R. W., Y. Yao, and X. L. Wang, 1997: Influence of the North American monsoon system on the U.S. summer precipitation regime. *J. Climate,* **10,** 2600–2622.

——, Y. Chen, and A. V. Douglas, 1999: Interannual variability of the North American warm season precipitation regime. *J. Climate,* **12,** 653–680.

——, W. Shi, and C. Hain, 2004: Relationships between Gulf of California moisture surges and precipitation in the southwestern United States. *J. Climate,* **17,** 2983–2997.

——, and Coauthors, 2006: The NAME 2004 field campaign and modeling strategy. *Bull. Amer. Meteor. Soc.,* **87,** 79–94.

Hoskins, B. J., and T. Ambrizzi, 1993: Rossby wave propagation on a realistic longitudinally varying flow. *J. Atmos. Sci.,* **50,** 1661–1671.

Hsu, H.-H., 2005: East Asian monsoon. *Intraseasonal Variability in the Atmosphere–Ocean Climate System,* K. M. Lau and D. E. Waliser, Eds., Springer-Verlag, 63–94.

Huffman, G. J., R. F. Adler, M. M. Morrissey, D. T. Bolvin, S. Curtis, R. Joyce, B. McGavock, and J. Susskind, 2001: Global precipitation at one-degree daily resolution from multisatellite observations. *J. Hydrometeor.,* **2,** 36–50.

Kawamura, R., T. Murakami, and B. Wang, 1996: Tropical and midlatitude 45-day perturbations during the northern summer. *J. Meteor. Soc. Japan,* **74,** 867–890.

Kiladis, G. N., and E. A. Hall-McKim, 2004: Intraseasonal modulation of precipitation over the North American monsoon region. *Proc. 15th Symp. on Global Change and Climate Variations,* Seattle, WA, Amer. Meteor. Soc., 11.4. [Available online at http://ams.confex.com/ams/pdfpapers/72428.pdf.]

Lau, K.-M., and P. H. Chan, 1986: Aspects of the 40–50 day oscillation during the northern summer as inferred from outgoing longwave radiation. *Mon. Wea. Rev.,* **114,** 1354–1367.

——, and H. Weng, 2002: Recurrent teleconnection patterns linking summertime precipitation variability over East Asia and North America. *J. Meteor. Soc. Japan,* **80,** 1309–1324.

Lau, N.-C., and M. J. Nath, 2006: ENSO modulation of the interannual and intraseasonal variability of the East Asian monsoon—A model study. *J. Climate,* **19,** 4508–4530.

Liebmann, B., and C. A. Smith, 1996: Description of a complete (interpolated) outgoing longwave radiation dataset. *Bull. Amer. Meteor. Soc.,* **77,** 1275–1277.

Livezey, R. E., and W. Y. Chen, 1983: Statistical field significance and its determination by Monte Carlo techniques. *Mon. Wea. Rev.,* **111,** 46–59.

Lorenz, D. J., and D. L. Hartmann, 2006: The effect of the MJO on the North American monsoon. *J. Climate,* **19,** 333–343.

Mesinger, F., and Coauthors, 2006: North American Regional Reanalysis. *Bull. Amer. Meteor. Soc.,* **87,** 343–360.

Mo, K. C., 2000: Intraseasonal modulation of summer precipitation over North America. *Mon. Wea. Rev.,* **128,** 1490–1505.

——, and R. W. Higgins, 1998: Tropical convection and precipitation regimes in the western United States. *J. Climate,* **11,** 2404–2423.

——, and J. Nogues-Paegle, 2005: Pan-America. *Intraseasonal Variability in the Atmosphere–Ocean Climate System,* K. M. Lau and D. E. Waliser, Eds., Springer-Verlag, 95–124.

Mullen, S. L., J. T. Schmitz, and N. O. Rennó, 1998: Intraseasonal variability of the summer monsoon over southeast Arizona. *Mon. Wea. Rev.,* **126,** 3016–3035.

Negri, A. J., R. F. Adler, E. J. Nelkin, and G. J. Huffman, 1994: Regional rainfall climatologies derived from Special Sensor Microwave Imager (SSM/I) data. *Bull. Amer. Meteor. Soc.,* **75,** 1165–1182.

Okabe, I. T., 1995: The North American monsoon. Ph.D. dissertation, University of British Columbia, 146 pp.

Sikka, D. R., and S. Gadgil, 1980: On the maximum cloud zone and the ITCZ over Indian longitudes during southwest monsoon. *Mon. Wea. Rev.,* **108,** 1840–1853.

Stensrud, D. J., R. L. Gall, and M. K. Nordquist, 1997: Surges over the Gulf of California during the Mexican monsoon. *Mon. Wea. Rev.,* **125,** 417–437.

Takaya, K., and H. Nakamura, 2001: A formulation of a phase-independent wave-activity flux for stationary and migratory quasigeostrophic eddies on a zonally varying basic flow. *J. Atmos. Sci.,* **58,** 608–627.

Tam, C.-Y., and N.-C. Lau, 2005: The impact of ENSO on atmospheric intraseasonal variability as inferred from observations and GCM simulations. *J. Climate,* **18,** 1902–1924.

Tang, M., and E. R. Reiter, 1984: Plateau monsoons of the Northern Hemisphere: A comparison between North America and Tibet. *Mon. Wea. Rev.,* **112,** 617–637.

Tian, B., I. M. Held, N.-C. Lau, and B. J. Soden, 2005: Diurnal cycle of summertime deep convection over North America: A satellite perspective. *J. Geophys. Res.,* **110,** D08108, doi:10.1029/2004JD005275.

Wang, B., and Q. Zhang, 2002: Pacific–East Asian teleconnection. Part II: How the Philippine Sea anomalous anticyclone is established during El Niño development. *J. Climate,* **15,** 3252–3265.

——, R. Wu, and K.-M. Lau, 2001: Interannual variability of Asian summer monsoon: Contrasts between the Indian and western North Pacific–East Asian monsoons. *J. Climate,* **14,** 4073–4090.